European Journal of Medicinal Chemistry 67 (2013) 90–97

Contents lists available at SciVerse ScienceDirect

European Journal of Medicinal Chemistry

journal homepage: http://www.elsevier.com/locate/ejmech

Original article

Synthesis, characterization and *in vitro* activity of thrombin-binding DNA aptamers with triazole internucleotide linkages

Anna M. Varizhuk [a,b,*], Vladimir B. Tsvetkov [c,d], Olga N. Tatarinova [a], Dmitry N. Kaluzhny [b], Vladimir L. Florentiev [b], Edward N. Timofeev [b], Anna K. Shchyolkina [b], Olga F. Borisova [b], Igor P. Smirnov [a], Sergei L. Grokhovsky [b], Anton V. Aseychev [a], Galina E. Pozmogova [a]

[a] Institute for Physical-Chemical medicine, Malaya Pirogovskaya Str., 1a, Moscow 119435, Russia
[b] Engelhardt Institute of Molecular Biology, Vavilov Str., 32 Moscow 119991, Russia
[c] Orekhovich Institute of Biomedical Chemistry, Pogodinskaya Str., 10, Moscow 119121, Russia
[d] Topchiev Institute of Petrochemical Synthesis, Leninsky Prospect, 29, Moscow 119991, Russia

ARTICLE INFO

Article history:
Received 18 February 2013
Received in revised form
11 June 2013
Accepted 14 June 2013
Available online 25 June 2013

Keywords:
Anticoagulants
Thrombin inhibition
DNA aptamers
G-Quadruplexes
Triazole internucleotide linkages

ABSTRACT

A series of DNA aptamers bearing triazole internucleotide linkages that bind to thrombin was synthesized. The novel aptamers are structurally analogous to the well-known thrombin-inhibiting G-quadruplexes TBA15 and TBA31. The secondary structure stability, binding affinity for thrombin and anticoagulant effects of the triazole-modified aptamers were measured. A modification in the central loop of the aptamer quadruplex resulted in increased nuclease resistance and an inhibition efficiency similar to that of TBA15. The likely aptamer-thrombin binding mode was determined by molecular dynamics simulations. Due to their relatively high activity and the increased resistance to nuclease digestion imparted by the triazole internucleotide linkages, the novel aptamers are a promising alternative to known DNA-based anticoagulant agents.

1. Introduction

DNA aptamers are increasingly recognized as drug candidates. Recently, DNA aptamers that bind to thrombin have emerged as potent inhibitors of thrombin function. These molecules are now extensively studied with respect to controlling blood clotting [1]. Currently available anticoagulants cause serious side effects, mainly due to low specificity or indirect action, and the development of new anticoagulants is of great importance due to the prevalence of cardiovascular disease. In the past two decades, a number of oligonucleotide-based thrombin inhibitors have been described [2–6], and two have entered clinical trials [7–9]. The two major problems limiting the application of the oligonucleotide aptamers to thrombin are rapid clearance from circulating blood and degradation by blood nucleases [10,11]. Rapid clearance may be advantageous in terms of tunability (reversibility) of the anticoagulation effect in a number of treatment options. However, it is important that the aptamers persist undigested for a period consistent with the desired dosing regimen. Chemical modifications (internucleotide, 2′-OMe, 2′-F and some other types) are commonly used to protect ONs from nucleases [12]. They are sometimes combined with bioconjugation (PEGylation in particular [12]) to improve pharmacokinetics and biodistribution of an aptamer, since nuclease resistance alone cannot dramatically increase its life span in blood.

The deoxyoligonucleotide TBA15 (thrombin binding aptamer), which forms an antiparallel two-tetrad G-quadruplex in solution, is the most efficient single-module unmodified DNA aptamer. Various modifications have been made to the TBA15 structure to improve its affinity to thrombin and its resistance to biodegradation [13–16]. Comparative analysis of known TBA15 analogs indicates that internucleotide modifications in the quadruplex loops are particularly promising [17–19]. Non-natural internucleotide linkages are likely to increase the biostability of aptamers [19,20].

Abbreviations: CD, circular dichroism; EDTA, ethylendiamine tetraacetic acid; EMSA, electrophoretic mobility shift assay; HPLC, high performance liquid chromatography; HR ES MS, high-resolution electrospray ionization mass spectrometry; MALDI TOF MS, matrix-assisted laser desorption/ionization-time of flight mass spectrometry; MD, molecular dynamics; MST, microscale thermophoresis; TBA, thrombin binding aptamer; Thr, thrombin; TLC, thin layer liquid chromatography; TT, thrombin time; XDA, X-ray diffraction analysis.

* Corresponding author. Institute for Physical-Chemical medicine, Malaya Pirogovskaya Str., 1a, Moscow 119435, Russia. Tel.: +7 (499) 2465470; fax: +7 (499) 2464409.
E-mail address: annavarizhuk@gmail.com (A.M. Varizhuk).

0223-5234/$ – see front matter © 2013 Elsevier Masson SAS. All rights reserved.
http://dx.doi.org/10.1016/j.ejmech.2013.06.034

Moreover, conformationally rigid linkages may restrict loop geometry in a manner that is favorable to specific aptamer activity. Triazole linkages are a type of rigid linkage and have been widely discussed due to their potential biocompatibility and pronounced effect on the hybridization properties of oligonucleotides [21–23].

In this study, we synthesized a series of DNA aptamers bearing triazole internucleotide linkages that bind to thrombin and assessed their stability, binding affinity for thrombin and anticoagulant effects.

2. Results and discussion

2.1. Synthesis and structure confirmation

We synthesized four analogs of TBA15 (A1-A4) in which triazole fragments were introduced into the central loop or in one or both TT loops and four analogs of 31TBA [24], a well-known double-module thrombin binding aptamer that contains a duplex fragment in addition to the quadruplex core (A5-A8). A5 and A7 carry triazole fragments in the duplex modules. A6 and A8 have modifications in TT loops (Fig. 1). Sequences of A5 and A6 are identical to that of 31TBA, while A7 and A8 has an 'inverted' duplex module and are generally similar to the recently reported 31TBA analog RE31 [24]. All of the modified aptamers were obtained via automated oligonucleotide synthesis using a modified dithymidine phosphoramidite block with a triazole internucleoside linkage. The modified phosphoramidite block was synthesized as described in Ref. [21].

According to CD spectroscopy (Fig. 2) and UV melting studies, all of the modified aptamers, with the exception of A7, fold into rather stable antiparallel G-quadruplexes. The UV melting curves can be found in Supplementary material, while the melting temperatures are presented in Table 1. The quadruplex module of A7 appeared to be unstable at room temperature. Interestingly, this dramatic decrease in the quadruplex melting temperature is caused by a modification in the duplex module. The quadruplex core is known to be essential for aptamer function; therefore, A7 was excluded from further investigations. The modification of the duplex module in aptamer A5 also caused destabilization, although this effect was less significant. The unfavorable effects of the introduction of triazole fragments into the duplex module are in agreement with recently published data on the hybridization properties of triazole-linked oligonucleotides. Modifications in one or both of the TT-loops (aptamers A1–A3, A6 and A8) had relatively insignificant effects on quadruplex thermostability, while modification of the central loop (A4) resulted in destabilization. It should be noted that we had to modify the sequence of the central loop in A4 to introduce the triazole fragment and the destabilization can be caused by the sequential change. All aptamers exhibited CD spectra that were generally similar to that of TBA15, with a positive band at 295 nm and a negative band at approximately 268 nm, which is characteristic of antiparallel quadruplexes. A hypochromic shift of the negative band and an increase in its amplitude was observed in the spectra of A4 and the double-module aptamers.

The monomolecular folding of the single-module aptamers was confirmed by comparing the UV melting curves obtained at different aptamer concentrations (see Supplementary material). No significant concentration dependence of the Tm values was observed. The monomolecular folding of A5–A8 was confirmed by rotational relaxation time analysis, in which the fluorescence polarization (P) and fluorescence lifetime (τ) of EtBr bound to the aptamers were measured, and the rotational relaxation time (ρ), which is proportional to the molecular hydrodynamic volume, was calculated. The obtained values for the rotational relaxation time are consistent with monomolecular folding (see Supplementary material).

2.2. Binding to thrombin

The binding affinity of the aptamers was analyzed by electrophoretic mobility shift assays (EMSA) (see Supplementary material). We labeled single-module aptamers with FAM for better visualization in these experiments. The affinities of A5 and A6 for thrombin were comparable to that of 31TBA. Other double-module aptamers demonstrated weak or no affinity for thrombin. EMSA data on the single-module aptamers were less clear. A4 was the only single-module aptamer which demonstrated significant binding. However, thrombin complexes with A4 and TBA15 are poorly seen on electropherograms, so for an accurate comparison we performed a microscale thermophoresis assay (MST) (Fig. 3). A K_D value of 97 nM ± 1 nM was determined for the TBA/Thr complex in the MST assay, in agreement with the value found in the literature [25]. The K_D value determined for A4 (127 nM ± 1.4 nM) was very close to that of TBA15. The addition of 10% blood plasma to the working buffer changed the K_D values significantly (K_D^{TBA} = 1690 nM ± 15 nM; K_D^{A4} = 3040 nM ± 65 nM), presumably due to unspecific interactions between the aptamers and plasma proteins, but the K_D^{TBA}/K_D^{A4} ratio remained below 2.

The thrombin-A4 binding mode was investigated by molecular dynamics (MD) simulations. The CD data indicate that the structure of A4 is generally close to that of TBA. Thus, we assumed that the two aptamers are likely to have similar patterns of interaction with thrombin, and our initial models of the A4/Thr complex were based on published data for the unmodified TBA/Thr complex (PDB: 1hao; PDB: 1hut). Two mutually inconsistent structures of the TBA/Thr complex have been reported: the NMR-resolved structure and the X-ray-resolved structure. In the NMR-based model (PDB: 1hao), TBA binds the Thr exosite-1 through the TT loops [26], while in the X-ray-based (XDA) model (PDB: 1hut), TBA binds through the TGT

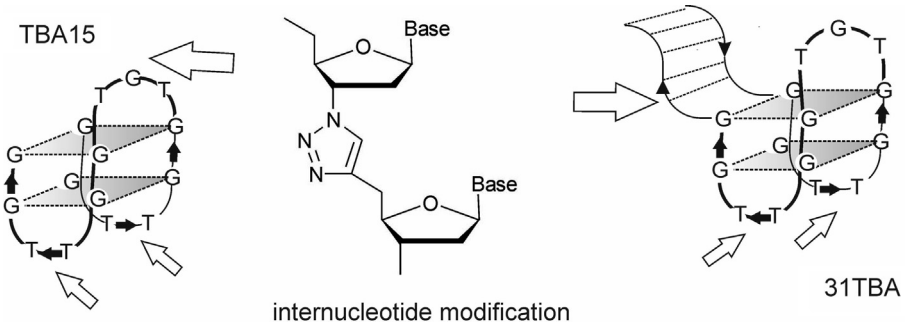

Fig. 1. Schematic representation of the thrombin binding aptamers TBA15 and 31TBA. The arrows indicate the modification positions. The modified dinucleoside fragment is shown in the center.

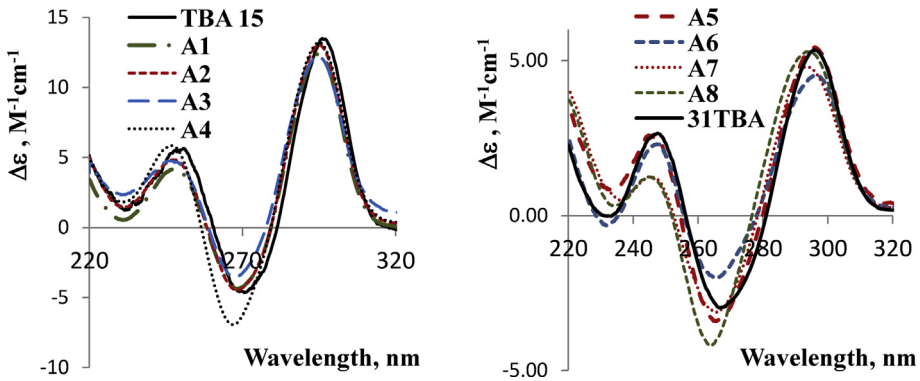

Fig. 2. CD spectra of single-module (left) and double-module (right) aptamers to thrombin.

loop [27]. The NMR model is known to be widely favored over the XDA model in the case of the unmodified TBA [28,29]. We decided to test the validity of both models with respect to the modified aptamer. To obtain the modified NMR- and XDA-resolved structures, we substituted the TGT loop of TBA in 1hao and 1hut correspondingly for the modified TT*T loop. After conformation reoptimization, MD simulations were performed for the A4/Thr complexes.

In the XDA model, the quadruplex geometry varied significantly. The quadruplex was completely destructed after 33 ns (Fig. 4A, B). Despite the quartet destruction, A4 remained bound to Thr throughout the simulation, mainly via G11, which forms H-bonds with Arg 73, and the T7T8 fragment, which forms H-bonds with Arg 70. The destabilization of the lower quartet was caused by shifting of the central loop, which resulted in stacking interactions between T8 and G6 as well as the formation of additional hydrogen bonds between the loop and Asp 6, Glu 155 and Ser 152. The gradual deformation of the quadruplex resulting in its destruction is illustrated in the gyration radius plots provided in the Supplementary material.

In the NMR model, the G-quadruplex was stable for at least 35 ns (Fig. 4C, D). The introduction of the triazole fragment did not cause any significant changes in the thrombin–aptamer interactions in this model. Similar to the unmodified aptamer, the A4 topology remained generally invariable throughout the simulation. The total number of hydrogen bonds between thrombin and A4 in the NMR model is greater than that in the XDA model. As in the XDA-model, Arg 70 and Arg 73 participate in hydrogen bond formation. Other amino acid residues that play a significant role are Tyr 71, Asp 74 and Tyr 114. The stacking interactions between T3 and Tyr 71 also contribute to thrombin–aptamer binding.

In conclusion, the MD results suggest that the NMR-based model is the only viable model for the A4/Thr complex. This finding is consistent with the profound impact of the triazole modification of the TT loops on aptamer binding to Thr and the relatively insignificant impact of the central loop modification (see the electrophoretic data in the Supplementary material and the MST data in Fig. 3).

2.3. Resistance to nuclease digestion and anticoagulant effects

The effect of the modification on biostability was assessed for aptamers A4, A5 and A6, which have proven promising in the thrombin binding assays. Despite its relatively high binding affinity, A6 later turned out to be an inefficient thrombin inhibitor (see below), so the data on its stability are presented merely to illustrate the sameness of loop modification effects in single-module and double-module aptamers. The direct evaluation of an aptamer life span in blood plasma can be problematic due to the complexity of its separation from plasma proteins. We confined our studies of aptamer biostability to DNaseI and S1 nuclease digestion assays. DNaseI is ubiquitous in human plasma and is believed to play a major role in oligonucleotide degradation. S1 was chosen as an example of a nuclease that primarily attacks single-stranded oligonucleotide fragments (quadruplex loops). Electrophoretic analysis of the hydrolysis rates of the aptamers is presented in Fig. 5 (The single module aptamers were FAM-labeled at 3′-

Table 1
Sequences, MALDI-TOF MS data and melting temperatures of the aptamers.

Aptamer code	Sequence[a], 5′→3′	*m/z*, found (calculated for $[M-H]^-$)	T_m, °C ± 1[b]
TBA15	GGTTGGTGTGGTTGG	4725.5 (4725.1)	52.6
A1	GGT*TGGTGTGGTTGG	4697.8 (4697.2)	50.5
A2	GGTTGGTGTGGT*TGG	4697.5 (4697.2)	48.9
A3	GGT*TGGTGTGGT*TGG	4668.9 (4669.2)	48.7
A4	GGTTGGTT*TGGTTGG	4673.0 (4672.2)	42.4
31TBA	CACTGGTAGGTTGGTGTGGTTGGGGCCAGTG	9708.5 (9709.3)	56.2
A5	CACT*TGTAGGTTGGTGTGGTTGGGGCAAGTG	9683.0 (9680.4)	42.3
A6	CACTGGTAGGTTGGTGTGGT*TGGGGCCAGTG	9685.7 (9681.4)	58.1
A7	GTGT*TGTAGGTTGGTGTGGTTGGGGCAACAC	9681.9 (9680.4)	25.2
A8	GTGACGTAGGTTGGTGTGGT*TGGGGCGTCAC	9682.5 (9681.4)	52.9

[a] Asterisks in the column 'Sequence' indicate triazole-modified internucleotide linkages.
[b] T_m values were measured at 295 nm in 20 mM Tris–HCl buffer (pH 7.5) containing 100 mM KCl.

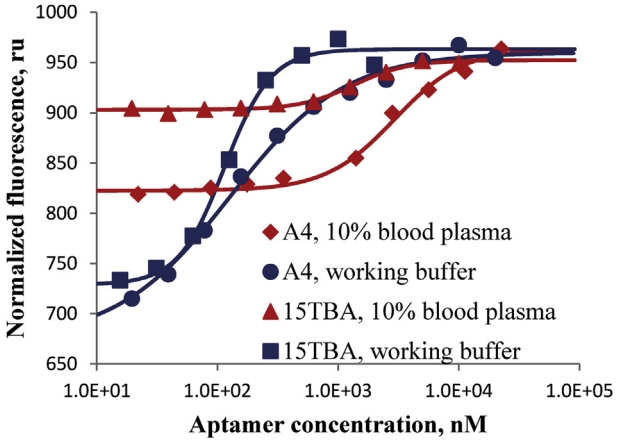

Fig. 3. TBA15 and A4 binding to thrombin. MST experimental values are fitted on the binding curve. Each value is an average of 3 measurements.

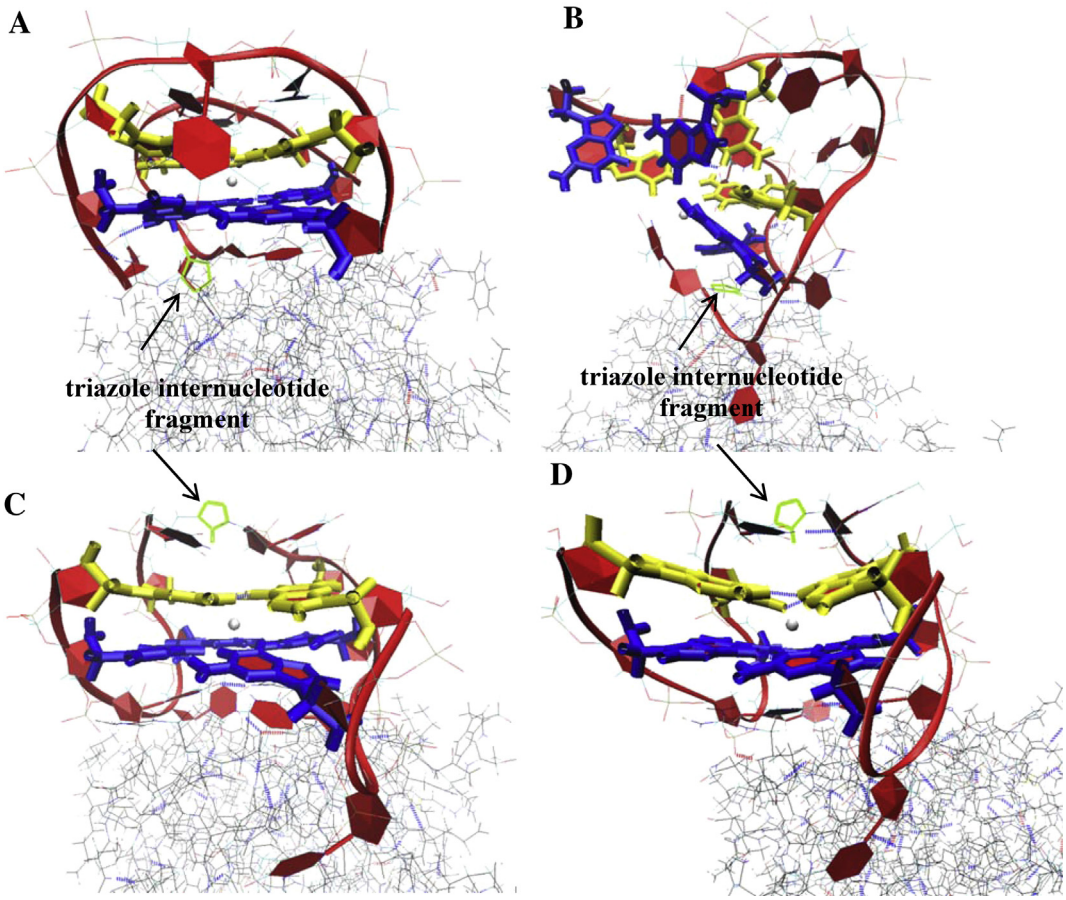

Fig. 4. MD simulation results. A, B – The XDA-based structure of the A4/Thr complex at simulation times of 1 ns and 35 ns, respectively. C, D – The NMR-based structure of the A4/Thr complex at simulation times of 1 ns and 35 ns, respectively. The triazole fragment is light green. (For interpretation of the references to color in this figure legend, the reader is referred to the web version of this article.)

terminus for better visualization in these experiments, so it should be noted that only 3′-terminal TBA15/A4 digestion fragments are seen in the electropherograms.). As evident from Fig. 5, modifications in quadruplex loops significantly increased aptamer resistance to S1 nuclease ($\tau_{1/2}^{A4,A6} \approx 10$ min, $\tau_{1/2}^{TBA15,TBA31} \approx 5$ min), but had a less pronounced effect on hydrolysis by DNaseI. Alternatively, modification in the duplex module protected the aptamer from DNaseI ($\tau_{1/2}^{A5} \approx 10$ min, $\tau_{1/2}^{TBA31} \approx 5$ min), but had little if any effect on hydrolysis by S1. This is probably because S1 nuclease preferentially attacks the quadruplex loops, while DNaseI appears to attack the duplex. The latter agrees with the observed dramatic difference between DNaseI hydrolysis rates of the single-module and double-module aptamers (TBA15 is 90% intact by the time 31TBA is fully digested. This can partially be attributed to the protective effect of the TBA15 3′-FAM label, but the protective effect of GQ-folding is most likely the major factor).

The anticoagulant effects of the modified aptamers were assessed using standard thrombin time tests. The thrombin activity was estimated based on the thrombin time values measured as a function of the aptamer concentration. The results are presented in Fig. 6. As illustrated in the figure, the inhibitory activities of A4, TBA15 and 31TBA were very similar ($IC_{50} \approx 250$ nM). The activity of A5 was slightly lower ($IC_{50} \approx 400$ nM), although still comparable with that of the unmodified aptamers. The increased resistance of the aptamers to nuclease activity and the anticoagulant effects of aptamers A4 and A5 indicate that they are potentially efficient anticoagulant agents.

3. Conclusion

The effects of triazole internucleotide modifications of the TBA15 loops and of the 31TBA duplex module on aptamer stability, binding affinity and inhibitory activity were studied. Rigid triazole fragments tended to disrupt aptamer function when introduced into the TT-loops or the duplex module, whereas the aptamer with a central loop modification retained its anticoagulant activity. Although the triazole modification failed to impart enhanced thrombin binding affinity to the aptamers, it protected them from nuclease digestion thus improving their biostability. Overall, two novel triazole-modified aptamers were proven to be potent thrombin inhibitors and could be used for the development of new anticoagulant drugs.

4. Experimental

4.1. Oligonucleotide synthesis, purification and MS analysis

ONs were synthesized on a Biosset ASM-800 DNA synthesizer following standard phosphoramidite protocols using standard commercial reagents and triazole-modified dinucleoside phosphoramidite. The only modification to the standard protocol was an increase in the coupling time to 15 min for the modified phosphoramidite block. The modified phosphoramidite block was synthesized as described in Ref. [23]. The structure and purity of the phosphoramidite were confirmed by HR ES MS, 31P NMR and TLC.

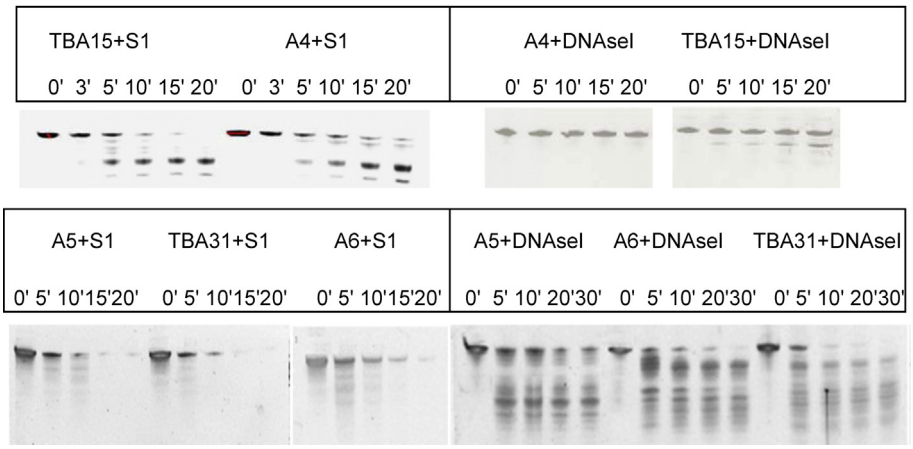

Fig. 5. The time course of aptamer hydrolysis by S1 nuclease and DNaseI.

All oligonucleotides were purified by preparative scale reverse-phase HPLC on a 250 mm × 4.0 mm Hypersil C18 column with detection at 260 nm and a 12–24% gradient of CH_3CN in 0.1 M ammonium acetate buffer. The dimethoxytrityl protection group was removed via treatment with 80% acetic acid (20 min), and the detritylated oligonucleotides were further purified in a 0–12% gradient of CH_3CN in 0.1 M ammonium acetate buffer. The purity of all oligonucleotides was determined to be ≥95% by HPLC. The MALDI TOF mass spectra of the oligonucleotides were acquired on a Bruker Microflex mass spectrometer in linear mode (+20 kV). Each spectrum was accumulated using 200 laser shots (N2 gas laser, 337 nm). A solution of 35 g/ml of 3-hydroxypicolinic acid with dibasic ammonium citrate was used as the matrix.

4.2. UV melting and CD

The oligonucleotides were dissolved in a 20 mM sodium phosphate buffer containing 100 mM KCl (pH 7.5). The oligonucleotide

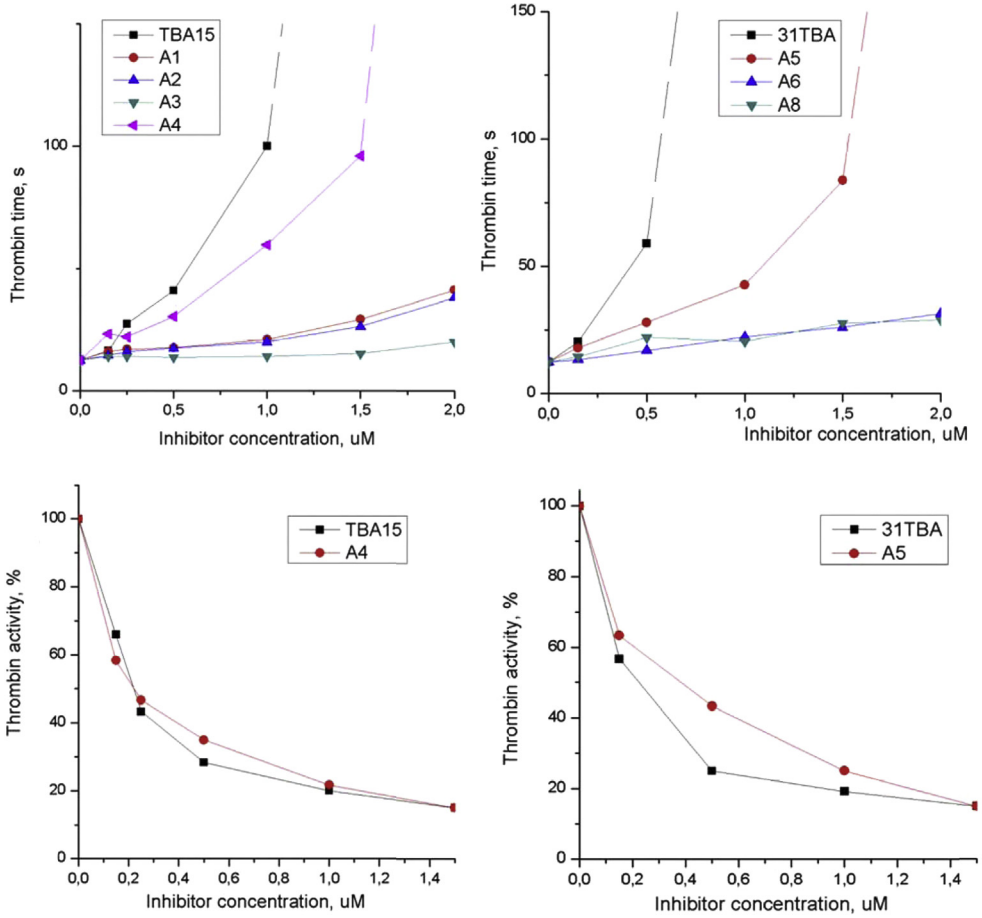

Fig. 6. The anticoagulant effects of single-module (left) and double-module (right) aptamers to thrombin. The thrombin time (TT) was measured in the presence of the aptamers and plotted as a function of the aptamer concentration (curves on the top). Each TT value is an average of three measurements. The TT values were converted into thrombin activity values (curves on the bottom) using a TT-activity calibration curve (see the Supplementary material).

single strand concentrations were calculated from the absorbance measured above 80 °C and the extinction coefficients, which were approximated using a nearest-neighbor model [30]. The samples were denatured at 95 °C for 5 min and snap cooled on ice prior to measurements to ensure monomolecular folding. The UV melting curves were recorded on a Jasco V-550 spectrophotometer equipped with a thermostated cuvette holder. The absorbance was registered at $\lambda = 295$ nm every 0.5 °C across the 15–90 °C temperature range. The melting temperatures of the quadruplexes were defined by performing a fitting procedure using the two-state model for monomolecular melting [31] in KaleidaGraph version 4.0. The circular dichroism (CD) spectra were obtained on a Jasco J-715 spectropolarimeter at 20 °C using samples annealed in the same buffer and under the same conditions as those used for the thermal denaturation studies. The CD values ($\Delta\varepsilon$) are given per mole of nucleotides in the quadruplex module.

4.3. Rotational relaxation time of EtBr bound to the aptamers

Vertical ($I_{||}$) and horizontal ($I_{\perp}$) components of the fluorescence of ethidium bromide (EtBr) bound to the aptamers were measured with a Cary Eclipse spectrofluorimeter at room temperature upon excitation by vertically polarized light. The excitation wavelength was 540 nm, and the fluorescence intensity was registered at 610 nm. The fluorescence polarization (P) was calculated as described in Ref. [32].

$$P = \left(I_{||} - I_{\perp}\right) \Big/ \left(I_{||} + I_{\perp}\right)$$

The free dye contribution was taken into account as described elsewhere [32]. Concentration of EtBr was 1 μM, oligonucleotide concentration was about 5 μM. Fluorescence lifetime (τ) of EtBr:TBA complexes was evaluated using Easy Life V. Fluorescence decay was registered using an RG610 long pass filter and LED excitation at 525 nm. Rotational relaxation time (ρ) was estimated using the Perrin–Weber equation, valid for small particles having spherical or low-asymmetrical ellipsoidal shape [33]:

$$\rho = 3\tau\left(\frac{1}{P_0} - \frac{1}{3}\right) \Big/ \left(\frac{1}{P} - \frac{1}{P_0}\right)$$

P is observed polarization, and $P_0 = 41 \pm 1\%$ is its limit value in the absence of rotational depolarization; and τ is fluorescence lifetime of EtBr in complexes with the aptamers.

4.4. EMSA

Preliminary analysis of thrombin binding by all aptamers was performed by electrophoretic mobility shift assay. Human α-thrombin was purchased from Sigma–Aldrich. All aptamers were annealed (heated to 95 °C and cooled quickly to room temperature) in 25 mM Tris–HCl buffer (pH 8) containing 100 mM KCl prior to the experiments. The aptamers were incubated with increasing concentrations of human α-thrombin for 15 min at room temperature in 25 mM Tris–HCl buffer (pH 8) containing 100 mM KCl, 5 mM $MgCl_2$ and 2 mM beta-mercaptoethanol in a total volume of 5 μL. The band shifts were resolved on a non-denaturing 8% polyacrylamide (19:1) gel in a Tris–HCl buffer (25 mM Tris–HCl, 10 mM KCl, 1 mM EDTA, pH 8.9). The concentration of aptamers A5–A8 and TBA31 in the probes was 2 μM. The corresponding gel was stained with SybrGreenII and analyzed using a GelDoc scanner (BioRad). Aptamers A1–A4 and TBA15 were FAM-labeled, and their concentration in the probes was 0.15 μM. The corresponding gel was analyzed using a Typhoon FLA 7000 scanner (GE Healthcare Lifesciences).

4.5. MST assay

A FAM-labeled aptamer (TBA or A4) was incubated for 15 min with human a-thrombin in 25 mM Tris–HCl buffer (pH 7.5) containing 150 nM NaCl, 5 mM KCl, 1 mM $CaCl_2$, 1 mM $MgCl_2$, 0.05% Tween 20 and 0.5 mg/mL BSA. The aptamers were used at a final concentration of 100 nM and annealed in working buffer without Tween-20 and BSA, as specified above, prior to the experiment. The thrombin concentration was varied from 0 to 25 μM. A 12-point dilution series was prepared for each aptamer. After incubation, the samples were loaded into MST standard-treated glass capillaries, and MST-analysis was performed using a Monolith NT.115 instrument (NanoTemper).

The above procedure was repeated with a working buffer containing 10% blood plasma. The plasma was obtained from 20 combined citrate-stabilized blood specimens from healthy individuals and stored at −20 °C until use. The samples containing blood plasma were centrifuged for 5 min at 12,000 g before loading into the capillaries.

4.6. Molecular dynamics

The molecular dynamics simulations (MD) were performed with the Amber 8 suite. The explicit (TIP3P) solvent simulations were performed in a cubic water box with periodic boundary conditions imposed. The parameters of all atoms with the exception of those of the triazole ring, needed for interatomic energy calculation, were taken from the force fields ff99SB and parmbsc0 [34]. The parameters of the triazole atoms were obtained using GAFF (general AMBER force field), and the triazole partial atomic charges were calculated with the quantum mechanical semi-empirical method PM3 [35] using the MOPAC 7.0 package included in Vega ZZ [36]. Two adjacent nucleotides on each side of the triazole fragment were taken into account when calculating the triazole parameters. A K^+ cation was placed in the center of the quadruplex between the quartets to stabilize the structure. The negative charges were neutralized by adding Na^+ ions, and approximately 7400 water molecules were employed for solvation. The structures were minimized prior to the simulations. First, the locations of the solvent molecules were optimized for 1000 steps (500 steps of a steepest descent minimization followed by 500 steps of a conjugate gradient minimization), with all the solute atoms being restrained to their positions with a force constant of 500 kcal mol^{-1} $Å^{-2}$. Then, the complex structure was optimized without any restriction for 2500 steps (1000 steps of steepest decent followed by 1500 steps of conjugate gradient). Subsequently, a gradual heating to 300 K over 20 ps was performed. To avoid wild fluctuations in the system at this stage, weak harmonic restraints with a force constant of 10 kcal mol^{-1} $Å^{-2}$ were used for all atoms with the exception of the solvent atoms. All bonds to hydrogen atoms were constrained using the SHAKE algorithm [37], which allowed a time step of 2 fs. The non-bound 1–4 van der Waals and electrostatic interactions were scaled by standard amber values (SCEE = 1.2, SCNB = 2.0). The cutoff for van der Waals interactions was set to 10 Å. Long-range electrostatics were calculated using the particle mesh Ewald method [38]. The MD simulations in a production phase were performed at $p = 1$ atm and $T = 300$ K under the control of a Langevin thermostat with a collision frequency of 1 ps^{-1}. The trajectory length was 35 ns. Snapshot visualization and hydrogen bond analysis were performed using VMD [http://www.ks.uiuc.edu/Research/vmd/] with a donor–acceptor distance of 3 Å and an angle cutoff of 20°. Snapshots were taken every 0.1 ns.

4.7. Nuclease hydrolysis

DNaseI and S1 nuclease were obtained from Fermentas. The aptamers were annealed in the reaction buffers prior to the

experiments as described above. In the DNaseI hydrolysis assay, 80 pmol of an aptamer was dissolved in 15 μL of a reaction buffer (10 mM Tris–HCl (pH 7.5), 25 mM $MgCl_2$ and 10 mM $CaCl_2$). A 2-μL aliquot was taken as a control, and 1 unit of DNaseI in 1 μL of storage buffer was added to the remaining solution. The mixture was incubated at 37 °C for 30 min. Aliquots were removed every 5–10 min and stored in a freezer at −20 °C until the end of the reaction. Once all the samples were collected, 1 μL of formamide was added to each sample. The samples were heated to 95 °C, then cooled on ice and loaded onto a denaturing 20% polyacrylamide gel for electrophoresis. The gel was run in TBE buffer (90 mM tris–borate (pH 8) and 20 mM EDTA), stained with SYBR Gold and analyzed using a GelDoc scanner (BioRad).

In the S1 hydrolysis assay, 80 pmol of an aptamer was dissolved in 15 μL of S1 working buffer (0.28 M NaCl, 0.05 M sodium acetate (pH 5) and 4.5 mM $ZnSO_4$). A 2-μL aliquot was taken as a control, and 10 unit of S1 nuclease was added to the remaining solution. Aliquots were taken every 5 min.

4.8. Thrombin time assay

The thrombin time (TT) was measured using the Renam Thrombin-TEST assay kit, following the published procedure [39] and the Renam protocols. Citrate-stabilized plasma was obtained as specified in the 'MST' section. The plasma (100 μL) was incubated for 120 s at 37 °C, and then thrombin (6 unit) and an aptamer were added to a final concentration of the latter 0.1–2 μM. The clotting time was then measured using a Unimed MiniLab-701 coagulation analyzer. To obtain the calibration curve for converting TT values to thrombin activity, a series of thrombin dilutions was prepared, and the thrombin times were measured (see the Supplementary material).

Acknowledgments

This work was supported by Russian Foundation for Basic Research [11-04-00131-a; 11-04-01544a; 11-04-02001a] and by the Program of the Presidium of the Russian Academy of Sciences on Molecular and Cell Biology.

Appendix A. Supplementary material

Supplementary material related to this article can be found at http://dx.doi.org/10.1016/j.ejmech.2013.06.034.

References

[1] R.C. Becker, T. Povsic, M.G. Cohen, C.P. Rusconi, B. Sullenger, Nucleic acid aptamers as antithrombotic agents: opportunities in extracellular therapeutics, Thromb. Haemostasis 103 (3) (2010) 586–595.
[2] D.M. Tasset, M.F. Kubik, W. Steiner, Oligonucleotide inhibitors of human thrombin that bind distinct epitopes, J. Mol. Biol. 272 (1997) 688–698.
[3] D.A. Di Giusto, G.C. King, Construction, stability, and activity of multivalent circular anticoagulant aptamers, J. Biol. Chem. 279 (45) (2004) 46483–46489.
[4] J. Muller, B. Wulffen, B. Potzsch, G. Mayer, Multidomain targeting generates a high-affinity thrombin-inhibiting bivalent aptamer, Chem. Bio Chem. 8 (2007) 2223–2226.
[5] Y. Kim, Z. Cao, W. Tan, Molecular assembly for high-performance bivalent nucleic acid inhibitor, Proc. Natl. Acad. Sci. U. S. A. 105 (2008) 5664–5669.
[6] K.M. Bompiani, D.M. Monroe, F.C. Church, B.A. Sullenger, A high affinity, antidote-controllable prothrombin and thrombin-binding RNA aptamer inhibits thrombin generation and thrombin activity, J. Thromb. Haemost. 10 (2012) 870–880.
[7] L.C. Bock, L.C. Griffin, J.A. Latham, E.H. Vermaas, J.J. Toole, Selection of single-stranded DNA molecules that bind and inhibit human thrombin, Nature 355 (1992) 564–566.
[8] L.C. Griffin, G.F. Tidmarsh, L.C. Bock, J.J. Toole, L.L.K. Leung, In vivo anticoagulant properties of a novel nucleotide-based thrombin inhibitor and demonstration of regional anticoagulation in extracorporeal circuits, Blood 81 (12) (1993) 3271–3276.
[9] G. Mayer, F. Rohrbach, B. Potzsch, J. Muller, Aptamer-based modulation of blood coagulation, Hämostaseologie 31 (2011) 258–263.
[10] W.A. Lee, J.A. Fishback, J.P. Shaw, L.C. Bock, L.C. Griffin, K.C. Cundy, A novel oligodeoxynucleotide inhibitor of thrombin. II. Pharmacokinetics in the cynomolgus monkey, Pharm. Res. 12 (1995) 1943–1947.
[11] H. Dougan, D.M. Lyster, C.V. Vo, A. Stafford, J.I. Weitz, J.B. Hobbs, Extending the lifetime of anticoagulant oligodeoxynucleotide aptamers in blood, Nucl. Med. Biol. 27 (2000) 289–297.
[12] J.M. Healy, S.D. Lewis, M. Kurz, R.M. Boomer, K.M. Thompson, C. Wilson, T.G. McCauley, Pharmacokinetics and biodistribution of novel aptamer compositions, Pharm. Res. 21 (12) (2004) 2234–2246.
[13] L. Bonifacio, F.C. Church, M.B. Jarstfer, Effect of locked-nucleic acid on a biologically active G-quadruplex. A structure–activity relationship of the thrombin aptamer, Int. J. Mol. Sci. 9 (2008) 422–433.
[14] T. Coppola, M. Varra, G. Oliviero, A. Galeone, G. D'Isa, L. Mayol, E. Morelli, M.-R. Bucci, V. Vellecco, G. Cirino, N. Borbone, Synthesis, structural studies and biological properties of new TBA analogues containing an acyclic nucleotide, Bioorg. Med. Chem. 16 (2008) 8244–8253.
[15] A. Avino, C. Fabrega, M. Tintore, R. Eritja, Thrombin binding aptamer, more than a simple aptamer: chemically modified derivatives and biomedical applications, Curr. Pharm. Des. 18 (14) (2012) 2036–2047.
[16] B. Sacca, L. Lacroix, J.-L. Mergny, The effect of chemical modifications on the thermal stability of different G-quadruplex-forming oligonucleotides, Nucleic Acids Res. 33 (2005) 1182–1192.
[17] A. Pasternak, F.J. Hernandez, L.M. Rasmussen, B. Vester, J. Wengel, Improved thrombin binding aptamer by incorporation of a single unlocked nucleic acid monomer, Nucleic Acids Res. 39 (3) (2011) 1155–1164.
[18] M. Zaitseva, D. Kaluzhny, A. Shchyolkina, O. Borisova, I. Smirnov, G. Pozmogova, Conformation and thermostability of oligonucleotide d(GGTTGGTGTGGTTGG) containing thiophosphoryl internucleotide bonds at different positions, Biophys. Chem. 146 (2010) 1–6.
[19] G. Pozmogova, M. Zaitseva, I. Smirnov, A. Shvachko, M. Murina, V. Sergeenko, Anticoagulant effects of thioanalogs of thrombin-binding DNA-aptamer and their stability in the plasma, Bull. Exp. Biol. Med. 150 (2) (2010) 180–184.
[20] G.X. He, J.P. Williams, M.J. Postich, S. Swaminathan, R.G. Shea, T. Terhorst, V.S. Law, C.T. Mao, C. Sueoka, S. Coutré, N. Bischofberger, In vitro and in vivo activities of oligodeoxynucleotide-based thrombin inhibitors containing neutral formacetal linkages, J. Med. Chem. 41 (22) (1998) 4224–4231.
[21] A.H. El-Sagheer, A.P. Sanzone, R. Gao, A. Tavassoli, T. Brown, Biocompatible artificial DNA linker that is read through by DNA polymerases and is functional in *Escherichia coli*, Proc. Natl. Acad. Sci. U. S. A. 108 (28) (2011) 11338–11343.
[22] H. Isobe, T. Fujino, N. Yamazaki, M. Guillot-Nieckowski, E. Nakamura, Triazole-linked analogue of deoxyribonucleic acid (TLDNA): design, synthesis, and double-strand formation with natural DNA, Org. Lett. 10 (2008) 3729–3732.
[23] A. Varizhuk, A. Chizhov, I. Smirnov, D. Kaluzhny, V. Florentiev, Triazole-linked oligonucleotides with mixed-base sequences: synthesis and hybridization properties, Eur. J. Org. Chem. 11 (2012) 2173–2179.
[24] A.V. Mazurov, E.V. Titaeva, S.G. Khaspekova, A.N. Storojilova, V.A. Spiridonova, A.M. Kopylov, A.B. Dobrovolsky, Characteristics of a new DNA aptamer, direct inhibitor of thrombin, Bull. Exp. Biol. Med. 150 (4) (2011) 422–425.
[25] P. Baaske, C.J. Wienken, P. Reineck, S. Duhr, D. Braun, Optical thermophoresis for quantifying the buffer dependence of aptamer binding, Angew. Chem. Int. Ed. 49 (2010) 1–5.
[26] K. Padmanabhan, A. Tulinsky, An ambiguous structure of a DNA 15-mer thrombin complex, Acta Crystallogr. 52 (1996) 272–282.
[27] K. Padmanabhan, K.P. Padmanabhan, J.D. Ferrara, J.E. Sadler, A. Tulinsky, The structure of alpha-thrombin inhibited by a 15-mer single-stranded DNA aptamer, J. Biol. Chem. 268 (1993) 17651–17654.
[28] R. Reshetnikov, A. Golovin, V. Spiridonova, A. Kopylov, J. Sponer, Structural dynamics of thrombin-binding DNA aptamer d(GGTTGGTGTGGTTGG) quadruplex DNA studied by large-scale explicit solvent simulations, J. Chem. Theory Comput. 6 (2010) 3003–3014.
[29] I.R. Krauss, A. Merlino, A. Randazzo, E. Novellino, L. Mazzarella, F. Sica, High-resolution structures of two complexes between thrombin and thrombin-binding aptamer shed light on the role of cations in the aptamer inhibitory activity, Nucleic Acids Res. 4016 (2012) 8119–8128.
[30] P.N. Borer, Optical properties of nucleic acids, absorption and circular dichroism spectra, in: , third ed.,, in: G.D. Fasman (Ed.), CRC Handbook of Biochemistry and Molecular Biology: Nucleic Acids, vol. 1 CRC Press, Cleveland, OH, 1975, pp. 589–595.
[31] L.A. Marky, K.J. Breslauer, Calculating thermodynamic data for transitions of any molecularity from equilibrium melting curves, Biopolymers 26 (1987) 1601–1620.
[32] G. Weber, S.R. Anderson, The effects of energy transfer and rotational diffusion upon the fluorescence polarization of macromolecules, Biochemistry 8 (1969) 361–371.
[33] A.K. Shchyolkina, O.F. Borisova, M.A. Livshits, G.E. Pozmogova, B.K. Chernov, R. Klement, T.M. Jovin, Parallel-stranded DNA with mixed AT/GC composition: role of trans G.C base pairs in sequence dependent helical stability, Biochemistry 39 (2000) 10034–10044.
[34] A. Perez, I. Marchan, D. Svozil, J. Sponer, T.E. Cheatham III, C.A. Laughton, M. Orozco, M. Refinement of the AMBER force field for nucleic acids:

improving the description of alpha/gamma conformers, Biophys. J. 92 (2007) 3817–3829.
[35] J.J.P. Stewart, Semiempirical molecular orbital methods, in: K.B. Lipkowitz, D.B. Boyd (Eds.), Reviews in Computational Chemistry, John Wiley & Sons, Inc., New York, 2007, pp. 45–81.
[36] A. Pedretti, L. Villa, G. Vistoli, VEGA – an open platform to develop chemo-bio-informatics applications, using plug-in architecture and script programming, J. Comput.-Aided Mol. Des. 18 (2004) 167–173.
[37] J.P. Ryckaert, G. Ciccotti, H.J.C. Berendsen, Numerical integration of the Cartesian equations of motion of a system with constraints: molecular dynamics of n-alkanes, J. Comput. Phys. 23 (1977) 327–341.
[38] T. Darden, D. York, L. Pedersen, Particle Mesh Ewald – an *N*.Log(*N*) method for Ewald sums in large systems, J. Chem. Phys. 98 (1993) 10089–10092.
[39] A. Clauss, Gerinnungsphysiologische Schnellmethode zur Bestimmung des Fibrinogens (Rapid physiological coagulation method in determination of fibrinogen), Acta Haematol. 17 (4) (1957) 237–246.